# Non-invasive Imaging of Atrial Flutter

M Seger[1], R Modre[2], B Pfeifer[1], C Hintermüller[1], B Tilg[1]

[1]University for Health Sciences, Medical Informatics and Technology, Hall in Tirol, Austria
[2]ARC Seibersdorf research GmbH, eHealth systems, Graz, Austria

## Abstract

*Non-invasive imaging of cardiac electrical function means – when talking about non-invasive imaging of cardiac electrophysiology (NICE) – to solve an ill-posed, nonlinear inverse problem. Due to the smoothing nature of the necessarily introduced spatial regularization term into the inverse problem formulation the reconstruction of especially atrial flutter shows up to be a major challenge.*

*This study clearly demonstrates, that imaging of atrial flutter employing the inverse reconstruction algorithm NICE is feasible and that the computed results correspond with invasively performed measurements.*

## 1. Introduction

Atrial and ventricular arrhythmias are of great concern in clinical electrocardiology [1, 2]. In clinical practice, the localization of the origins of arrhythmias is currently achieved by traditional catheter techniques and by catheter mapping techniques [1, 3]. These methods show significant limitations when talking about acquiring single-beat activation maps. In addition, the invasive interventions cannot be used for monitoring patients in order to decide the optimal individual curative therapy (e. g., drug, ablative or hybrid therapy). The simultaneous acquisition of three-dimensional (3D) anatomical and electrocardiographic (ECG) data of individual patients enables noninvasive imaging of the human cardiac function. Three-dimensional anatomical data from the human thorax can be obtained, e. g., from magnetic resonance imaging (MRI), ECG data can be acquired from the patient's chest surface employing, e.g., multichannel (32 up to 256 channels) biopotential recording systems. The coupling of these two modalities in time and space permits the imaging of electrical function when bioelectromagnetical field theory is applied and when an *ill-posed inverse problem* can be solved [4, 5, 6, 7]. The primary electrical source – according to the bidomain theory [8] – in the cardiac muscle is the spatio-temporal distribution of the *transmembrane potential* (TMP) $\varphi_m$ [4, 5, 9]. The potential on the chest surface and the potential on all other conductivity interfaces are related to $\varphi_m$ by a *Fredholm integral equation* of second kind. The relationship between the impressed electrical sources and the potentials at the electrode sites on the torso surface can mathematically be described by the *leadfield-* or also termed *transfer-matrix*, which is the solution of the *forward problem of electrocardiography* [4, 10]. The boundary element method (BEM) – a surface integral equation approach – can, in general, be applied to solve this forward problem [4, 5, 11]. In the *electrocardiographic inverse problem*, the electrical source distribution is reconstructed from the body surface maps employing an electrical source model description. Because of the generally unknown individual cardiac fiber orientation, *electrical isotropy* is assumed in the surface heart model approach based on the *bidomain theory* [5, 6, 7]. The most established inverse formulations are the imaging of the *activation time* (AT) map on the entire surface of the atria or ventricles (epi- and endocardial surfaces), like, e.g., Non-invasive Imaging of Cardiac Electrophysiology (NICE) [7, 12, 13, 14], and the imaging of the *epicardial potential pattern* [15, 16]. The AT imaging approach looks for the time of onset of depolarization at each source node, whereas the epicardial potential problem aims at estimating the (extracellular) potential on the pericardium. When used in a straightforward manner, the epicardial potential formulation does not allow imaging of the potentials on the endocardia. The heart model approach employing the bidomain theory, however, is capable of imaging the electrical excitation on the entire atrial or ventricular surface, i. e., on the epicardium as well as on the endocardia. This is of particular interest from a clinical point of view, as most of the catheter interventions in the electrophysiology (EP) lab are performed on the endocardia.

Imaging and localizing the origin of cardiac focal events, like, e.g., extrasystoles, ventricular preexcitation, but also reconstruction of more complex activation patterns, like, e.g., sinus rhythm, has been performed with appropriate accuracy employing NICE. The current study investigates, whether it is also possible to image more sophisticated cardiac arrhythmias, like atrial flutter applying NICE.

## 2. Methods

One patient (55 years, male) suffering from atrial flutter circling around the tricuspid annulus was interventionally treated by radiofrequency catheter ablation with the electroanatomic-mapping system CARTO™(Biosense Webster Inc.) at the Department of Cardiology of the Medical University Innsbruck, Austria. Written informed consent was obtained from the patient before any diagnostic and therapeutic treatment. The study was approved by the local ethics committee. The inverse estimation of atrial activation times of both atria was organized as follows: Previous to the intervention, the patient was moved to the MRI scanner. Afterwards, the volume conductor model consisting of the lungs, chest surface, blood masses and the atria was generated.

**MRI scanning** An MRI scan of the patient was made previous to the intervention. The individual anatomical data was obtained from MRI using a Magnetom-Vision-Plus 1.5 T (Siemens Medical Solutions) scanner. The atrial geometry was recorded in CINE-mode during breath-hold (expiration, short-axis scans, 6 mm spacing). The shape of the lungs and the torso were recorded in T1-FLASH-mode during breath-hold (expiration, long-axis scans, 10 mm spacing). Seven markers (vitamin E-capsules, anatomical landmarks on the anterior and lateral chest wall) were used to couple the locations of the electrodes to the MRI frame. Eleven capsules were attached on the back, in order to tag the positions of the posterior electrodes, which were not accessible during the EP study.

**Generation of the Volume Conductor Model** The volume conductor model containing the relevant compartments (i. e., atria, chest surface, lungs, blood masses) of the individual patient was generated using the software package amiraDev™ 3.0 (TGS Europe Inc.) in combination with a semi-automatic myocardial extraction tool [17]. The lungs and chest could be segmented in a straightforward manner. A marching cubes algorithm was applied to the segmented compartments, which resulted in a triangulated surface mesh of the whole volume conductor model. The extracted volume conductor model is depicted in Fig. 1.

When the patient arrived in the EP lab, the posterior, lateral and anterior electrodes were attached on the patient's chest in order to record the body surface potential (BSP) map. The positions of the anterior and lateral electrodes were digitized using the Fastrak system (Polhemus Inc.). Additionally, the locations of the 7 anatomical landmarks were digitized in order to allow transformation into the MRI frame. The computation of the leadfield-matrix and of the ATs, respectively, was performed on an INTEL Xeon™dual processor (2.8 GHz with 2 GB memory for each processor).

**Computation of the leadfield-matrix** After transformation of the electrode coordinates into the MRI frame, the leadfield-matrix was computed. The leadfield-matrix $\mathbf{L}$ with dimension e $\times$ s describes the relationship between the impressed electrical sources and the (extracellular) potentials $\mathbf{\Phi}$ in e electrodes for all time steps T [4, 10]:

$$\mathbf{\Phi} = \mathbf{L}\mathbf{\Phi_m}, \tag{1}$$

with the s $\times$ T matrix $\mathbf{\Phi_m}$ containing the TMPs (electrical sources) in all s nodes of the cardiac surface. Note that $\mathbf{\Phi_m}$ is the time-discretized expression of $\varphi_m$. The computation of $\mathbf{L}$ was performed applying the BEM. The isotropic conductivity values for the different compartments were chosen according to [4]: ventricles: effective intracellular conductivity: 0.1 $\mathrm{Sm}^{-1}$, bulk conductivity: 0.2 $\mathrm{Sm}^{-1}$; lungs: 0.08 $\mathrm{Sm}^{-1}$, blood masses: 0.6 $\mathrm{Sm}^{-1}$, and chest: 0.2 $\mathrm{Sm}^{-1}$.

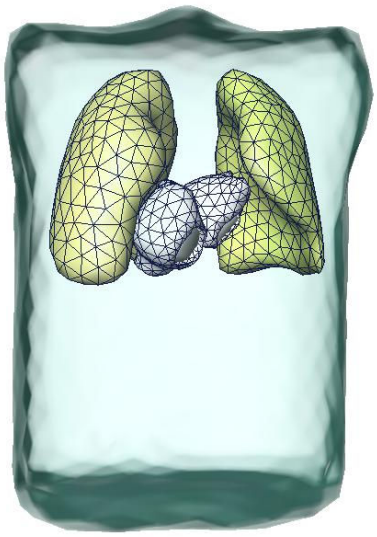

Figure 1. Volume conductor model of the patient suffering from atrial flutter displayed in a anterior-posterior view. The model comprises both atria, the corresponding blood masses (located within the atrial chambers), left and right lung and the torso surface.

**Acquisition of the BSP Map** The ECG mapping data was recorded before, during and after the EP study. The BSP map was acquired in 62 channels by the Mark-8 system (Biosemi V.O.F.). The Wilson-Central-Terminal (WCT) defined the reference potential [18]. The sampling rate was 2048 Hz. Signals were bandpass filtered with a lower and upper edge frequency of 0.3 and 400 Hz, respectively. The AC-resolution of the system was 500 $\mathrm{nVbit}^{-1}$ (16 bits per channel).

**Signal preprocessing** For estimating the AT pattern, the ECG signals representing the atrial depolarization sequences (target ECG waves) were used as input for fur-

ther computation. In case of imaging atrial flutter, the red colored wave in Fig. 2 (right upper panel) indicates the chosen target wave duration (this wave represents Wilson chest lead V1). The extracted signals of all electrodes were baseline corrected and no additional filtering was applied. The time discretization interval was set 1 ms.

**Estimation of the AT on the Heart Surface** The estimation of the ATs by considering (1) and (2) leads to an ill-posed, nonlinear (the TMP $\varphi_{\mathbf{m}}(\mathbf{t})$ depends nonlinearly on the AT $\tau$ [6]), inverse problem. Because of the ill-posedness, *regularization techniques* have to be employed in order to guarantee a stable solution in the presence of modeling errors and measurement noise. As the AT imaging focuses on the estimation of the time of onset of *depolarization*, the time course of the TMP at each source point of the atrial surface can be approximated employing the analytical formula [6]

$$\varphi_m(\tau, t) = \frac{u}{2}\left\{1 + \frac{2}{\pi}\arctan\left[\pi\frac{t-\tau}{w}\right]\right\} + a, \qquad (2)$$

where a represents the resting transmembrane potential ($a$ = – 90 mV), $u$ the action potential amplitude ($u$ = 100 mV) and $w$ the rise time $w$ = 2 ms. Equation (2) determines the TMP time course and can therefore be considered as *temporal regularization*. Spatial regularization is achieved by adding the surface Laplacian [19] in the cost function [6, 7], which is to be optimized with respect to $\tau$

$$\|\mathbf{L}\mathbf{\Phi}_{\mathbf{m}} - \mathbf{D}\|_{\mathbf{F}}^{\mathbf{2}} + \lambda^{\mathbf{2}}\|\mathbf{\Delta}\tau\|^{\mathbf{2}} \longrightarrow \text{ min.} \qquad (3)$$

The surface Laplacian $\Delta$ is introduced in (3) in order to avoid an unphysiological AT pattern by smoothing the solution of the AT map. Parameter $\lambda$ determines the amount of regularization and is calculated employing the *L-curve method* [20], weighting the residual norm on the left hand side of (3) against the spatial regularization term. The e $\times$ T matrix $\mathbf{D}$ contains the measured (time discrete) ECG data in the electrodes and $\|\cdot\|_F$ represents the Frobenius norm. The interval [0, T] reflects the duration of depolarization of the underlying target ECG wave. A Quasi-Newton solver was used for minimizing the functional in (3).

**Validation of the computed AT map** The computed AT map was compared with conventional ECG diagnosis and with the CARTO map, respectively. After the intervention had been finished, the position of the 7 anatomical markers were digitized with the ablation catheter, in order to allow transformation of the CARTO map and the catheter ablation points into the MRI frame.

## 3. Results

The corresponding AT maps found with the CARTO system and the AT maps computed by NICE are displayed in Fig. 2. The CARTO AT map is superimposed onto the atrial geometry (transparent style) extracted and segmented from the MRI data. The counter-clockwise rotation of the flutter circle around the tricuspid annulus could be properly reconstructed. Note that the AT maps generated by CARTO only cover the right atrium (no clinical indication for mapping also the left atrium), whereas NICE is capable of reconstructing the electrical ATs of both atria on the endocardia and epicardium simultaneously.

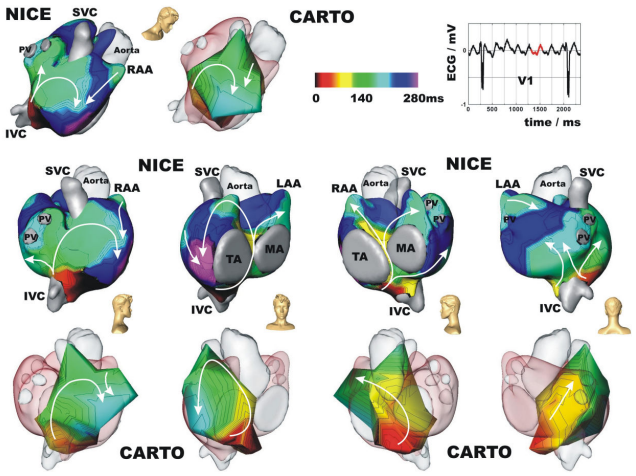


Figure 2. Activation times of a patient suffering from atrial flutter circling around the tricuspid annulus. The underlying target ECG-wave (Wilson Lead V1) used for reconstructing the activation times employing the Non-invasive Imaging of Cardiac Electrocardiophysiology (NICE) is shown in the right upper panel. The color coded activation times (red...early, blue-velvet...late activation) computed by NICE are compared with the invasively measured activation times by the CARTO$^{TM}$system (CARTO maps superimposed on the MRI atrial geometry) displayed for five different views (note the head icon helping for spatial orientation).

## 4. Discussion and conclusions

Non-invasive imaging of atrial flutter is feasible even under clinical conditions. The corresponding ECG signals, however, do not show high potential amplitudes (see Fig. 2 right upper row). Additionally, no electrical isoline can be observed, which has a negative influence on the ECG signal-preprocessing task. The high activation time gradients of areas, where the wavefront starts and ends nearby, make it also difficult for NICE to properly reconstruct the excitation process. This fact is due to the spatial regularization of the inverse problem, which is, however, necessary to guarantee unphysiological breakthroughs as well as unphysiological AT patterns. Thus the NICE reconstruc-

tion algorithm should be modified in case of imaging atrial flutter: The target ECG-wave, which was used for reconstructing the underlying cardiac excitation process, could be shifted in time and the AT map was recomputed and averaged. Another approach could be to integrate the, e.g., epicardial potential estimation or transmembrane reconstruction algorithm, whose results would be interactively imposed onto the computed ATs by NICE as side constraints, thus enabling subsumed faster computation times at an appropriate and clinically acceptable level of accuracy.

## Acknowledgements

This study was funded by the START Y144-N04 program granted by the Austrian Federal Ministry of Education, Science and Culture (bm:bwk) in collaboration with the Austrian Science Fund (FWF).

The authors are grateful with the Department of Cardiology of the Medical University Innsbruck, especially with Prof. Dr. Pachinger and Dr. Hintringer for their effort and support with respect to the clincal studies.

## References

[1] Lesh M D, Kalman J M, Olgin J E, Ellis W S. The role of atrial anatomy in clinical atrial arrhythmias. Journal of Electrocardiology 1996;29:101–113.

[2] SippensGroenewegen A, Lesh M D, Roithinger F X, Ellis W S, Steiner P R, Saxon L A, Lee R J, Scheinman M M. Body surface mapping of counterclockwise and clockwise typical atrial flutter: A comparative analysis with endocardial activation sequence mapping. Journal of the American College of Cardiology 2000;35(5):1276–1287.

[3] Ben Haim S A, Osadchy D, Schuster I, Gepstein L, Haya G, Josephson M E. Nonfluoroscopic, in vivo navigation and mapping technology. Nature Medicine 1996;2:1393–1395.

[4] Fischer G, Tilg B, Modre R, Huiskamp G J M, Fetzer J, Rucker W, Wach P. A bidomain model based BEM–FEM coupling formulation for anisotropic cardiac tissue. Annals of Biomedical Engineering 2000;28(10):1229–1243.

[5] Greensite F. The mathematical basis for imaging cardiac electrical function. Critical Reviews in Biomedical Engineering 1994;22:347–399.

[6] Modre R, Tilg B; Fischer G, Wach P. Noninvasive myocardial activation time imaging: a novel inverse algorithm applied to clinical ECG mapping data. IEEE Transactions on Biomedical Engineering 2002;49(10):1153–1161.

[7] Tilg B, Fischer G, Modre R, Hanser F, Messnarz B, Schocke M, Kremser C, Berger T, Hintringer F, Roithinger F X. Model-based imaging of cardiac electrical excitation in humans. IEEE Transactions on Medical Imaging 2002;21(9):1031–1039.

[8] Geselowitz D B, Miller 3rd W T. A bidomain model for anisotropic cardiac muscle. Annals of Biomedical Engineering 1983;11(3–4):191–206.

[9] Henriquez C. S. Simulating the electrical behavior of cardiac tissue using the bidomain model. Critical Reviews in Biomedical Engineering 1993;21(1):1–77.

[10] Mosher J C, Leahy R M, Lewis P S. Eeg and meg: Forward solutions for inverse methods. IEEE Transactions on Biomedical Engineering 1999;46(3):245–259.

[11] Huiskamp G, van Oosterom A. The depolarization sequence of the human heart surface computed from measured body surface potentials. IEEE Transactions on Biomedical Engineering 1988;35:1047–1058.

[12] Modre R, Tilg B, Fischer G, Hanser F, Messnarz B, Seger M, Hintringer F, Roithinger F X. Ventricular surface activation time imaging from electrocardiogram mapping data. Medical and Biological Engineering and Computing 2004;42(2):146–150.

[13] Modre R, Tilg B, Fischer G, Hanser F, Messnarz B, Seger M, Schocke M, Berger T, Hintringer F, Roithinger F X. Atrial noninvasive activation time imaging of paced rhythm data. Journal of Cardiovascular Electrophysiology 2003;14(7):712–719.

[14] Tilg B, Hanser F, Modre R, Fischer G, Messnarz B, Berger T, Hintringer F, Pachinger O, Roithinger F X. Clinical ECG mapping and imaging of cardiac electrical excitation. Journal of Electrocardiology 2002;35(Suppl):81–87.

[15] Oster H S, Taccardi B, Lux R L, Ershler P R., Rudy Y. Noninvasive electrocardiographic imaging: Reconstruction of epicardia potentials, electrograms and isochrones and localization of single and multiple electrocardiac events. Circulation 1997;96:1012–1024.

[16] Burnes J E, Taccardi B, Rudy Y. A noninvasive imaging modality for cardiac arrhythmias. Circulation 2000; 102(17):2152–2158.

[17] Pfeifer B, Fischer G, Hanser F, Seger M, Hintermueller C, Modre - Osprian R, Trieb T, Tilg B. Atrial and ventricular myocardium extraction using model based techniques. Methods of Information in Medicine 2006;45:19–26.

[18] Fischer G, Tilg B, Wach P, Modre R, Hanser F, Messnarz B. On modelling the Wilson terminal in the boundary and finite element method. IEEE Transactions on Biomedical Engineering 2002;49(3):217–224.

[19] Huiskamp G J. Difference formulas for the surface laplacian on a triangulated surface. Journal of Computational Physics 1991;95:477–496.

[20] Hansen P C. Computational Inverse Problems in Electrocardiography. WIT Press, Southampton, 2001; 119–142.

Address for correspondence:

Michael Seger
Eduard-Wallnöfer-Zentrum 1, A-6060 Hall in Tirol
michael.seger@umit.at